

Article

Encapsulated Ni@La₂O₃/SiO₂ Catalyst with a One-Pot Method for the Dry Reforming of Methane

Luhui Wang ^{1,*} , Rong Hu ^{1,2}, Hui Liu ³, Qinhong Wei ¹, Dandan Gong ¹, Liuye Mo ⁴, Hengcong Tao ¹ and Zhonghuai Zhang ¹

¹ Department of Chemical Engineering, School of Petrochemical Technology and Energy Engineering, Zhejiang Ocean University, Zhoushan 316022, Zhejiang, China; hurongzjou2017@126.com (R.H.); weiqinhong@zjou.edu.cn (Q.W.); dandangong@zjou.edu.cn (D.G.); hengcongtao@zjou.edu.cn (H.T.); zhang012138@126.com (Z.Z.)

² School of Naval Architecture and Mechanical-electrical Engineering, Zhejiang Ocean University, Zhoushan 316022, Zhejiang, China

³ School of Food and Pharmaceutical, Zhejiang Ocean University, Zhoushan 316022, Zhejiang, China; liuhui@zjou.edu.cn

⁴ Institute of Innovation & Application, Zhejiang Ocean University, Zhoushan 316022, Zhejiang, China; liuyemo@zjou.edu.cn

* Correspondence: wangluhui1008@zjou.edu.cn; Tel.: +86-580-255-1050

Received: 22 November 2019; Accepted: 25 December 2019; Published: 28 December 2019

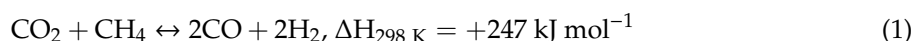


Abstract: Ni nanoparticles encapsulated within La₂O₃ porous system (Ni@La₂O₃), the latter supported on SiO₂ (Ni@La₂O₃/SiO₂), effectively inhibit carbon deposition for the dry reforming of methane. In this study, Ni@La₂O₃/SiO₂ catalyst was prepared using a one-pot colloidal solution combustion method. Catalyst characterization demonstrates that the amorphous La₂O₃ layer was coated on SiO₂, and small Ni nanoparticles were encapsulated within the layer of amorphous La₂O₃. During 50 h of dry reforming of methane at 700 °C and using a weight hourly space velocity (WHSV) of 120,000 mL g_{cat}⁻¹ h⁻¹, the CH₄ conversion obtained was maintained at 80%, which is near the equilibrium value, while that of impregnated Ni–La₂O₃/SiO₂ catalyst decreased from 63% to 49%. The Ni@La₂O₃/SiO₂ catalyst exhibited very good resistance to carbon deposition, and only 1.6 wt% carbon was formed on the Ni@La₂O₃/SiO₂ catalyst after 50 h of reaction, far lower than that of 11.5 wt% deposited on the Ni–La₂O₃/SiO₂ catalyst. This was mainly attributed to the encapsulated Ni nanoparticles in the amorphous La₂O₃ layer. In addition, after reaction at 700 °C for 80 h with a high WHSV of 600,000 mL g_{cat}⁻¹ h⁻¹, the Ni@La₂O₃/SiO₂ catalyst exhibited high CH₄ conversion rate, ca. 10.10 mmol g_{Ni}⁻¹ s⁻¹. These findings outline a simple synthesis method to prepare supported encapsulated Ni within a metal oxide porous structure catalyst for the dry reforming of methane reaction.

Keywords: Ni; La₂O₃; colloidal solution combustion; dry reforming of methane; carbon deposition

1. Introduction

Dry reforming of methane (DRM) is a promising process, as it can simultaneously convert CO₂ and CH₄ present in CO₂-rich natural gas reservoirs to produce syngas. The latter serves as the raw material to produce liquid fuels through gas-to-liquid technology (via Fischer–Tropsch synthesis) [1]. Due to the strong endothermic nature of the DRM reaction, most of previous studies were conducted at temperatures higher than 600 °C for high conversions of CO₂ and CH₄. Therefore, developing a robust catalyst that possesses good stability and excellent resistance to coke plays a crucial role in the DRM reaction [2–4].



Many catalysts have been investigated for the DRM reaction. As a result, precious-metals-based catalysts, for instance, Ru, Rh, Pd, Ir, Pt, etc., exhibited good catalytic activity and stability. However, the disadvantage of using noble-metals-based catalysts is their high cost [5–7]. Ni-based catalysts, due to good catalytic activity and low cost, have been widely investigated for the DRM reaction [8–10]. However, Ni-based catalysts are prone to carbon deposition and metal sintering during DRM [11,12]. Designing a DRM catalyst that resists against carbon deposition and metal sintering could be accomplished by making appropriate choice of support, promoter, structure, and methods of preparation [2–4]. Because oxygen species in the CeO₂ lattice can effectively lower carbon accumulation by oxidation of accumulated carbon, various Ni/CeO₂ compositions were extensively studied to prevent carbon deposition [13–16]. In addition, small metallic Ni nanoparticles more effectively inhibit the nucleation and growth of coke, thereby restraining coke deposition on the catalyst [17,18]. Ni particles, smaller than 5 nm, can effectively reduce carbon deposition [15,18–21]. Small Ni particles also have poor thermal stability, especially at high reaction temperatures. Encapsulated Ni-based catalysts [22–27], such as core-shell Ni@SiO₂ [28–30], were used to suppress carbon deposition and enhance the stability of small Ni particles in the DRM reaction. Sandwiched SiO₂@Ni@CeO₂ [31] and SiO₂@Ni@ZrO₂ [32] catalysts were applied for the DRM, exhibiting high catalytic activity and excellent coke resistance. However, encapsulated catalysts usually require complex preparation processes. The development of a simple method for preparing encapsulated Ni-based catalyst is thus required.

As La₂O₃ can promote CO₂ adsorption and activation [33]; Ni/La₂O₃ [34,35] and La₂O₃ promoted Ni-based catalysts [36–39] have shown excellent activity in the DRM reaction. However, due to the low specific surface area of La₂O₃, the main problem with Ni/La₂O₃ catalysts is the poor dispersion of Ni [40,41], leading to carbon deposition on Ni/La₂O₃ catalysts [40,41]. Li et al. [42] reported ordered mesoporous Ni/La₂O₃ catalysts with large specific surface area for DRM, and the experimental result indicated that the increased interface between Ni and La₂O₃ is beneficial for suppressing carbon deposition.

A colloidal solution combustion method has been reported to prepared mesoporous CeO₂ [43]. In this study, a novel Ni@La₂O₃/SiO₂ catalyst was prepared via one-pot synthesis using the colloidal solution combustion method. For the Ni@La₂O₃/SiO₂ catalyst, small Ni particles were encapsulated within an amorphous La₂O₃ layer and supported on SiO₂. The prepared Ni@La₂O₃/SiO₂ catalyst has an abundant interface between Ni and La₂O₃, which was more active and stable compared to the Ni–La₂O₃/SiO₂ catalyst prepared using the standard impregnation method.

2. Results and Discussion

2.1. Characterization of Fresh and Reduced Catalysts

The N₂ adsorption results of the Ni@La₂O₃/SiO₂ and Ni–La₂O₃/SiO₂ catalysts are listed in Table 1. The specific surface area (S_{BET}) of the Ni@La₂O₃/SiO₂ is 19.0 m² g^{−1}, which is smaller than that of the Ni–La₂O₃/SiO₂ catalyst. The pore volume and average pore size of Ni@La₂O₃/SiO₂ catalyst are 0.21 cm³ g^{−1} and 43.9 nm, respectively, which are larger than those of Ni–La₂O₃/SiO₂ catalyst.

It is noted that the Ni@La₂O₃/SiO₂ catalyst has a significantly lower specific surface area compared with the recently reported mesoporous Ni–La₂O₃ (172 m²·g^{−1}) [42] and Ni–La₂O₃/SiO₂ (190 m² g^{−1}) [38] catalysts for DRM. In our previous report [43], mesoporous Ni–La₂O₃ (70.4 m² g^{−1}) had been synthesized by the same colloidal solution combustion method with colloidal SiO₂ as a template, and the silica was then removed by NaOH etching to form mesopores. Compared with our previously reported mesoporous Ni–La₂O₃ catalysts, the Ni@La₂O₃/SiO₂ catalyst may be more suitable for high-temperature reactions due to the use of silica as support of La₂O₃ and Ni.

Table 1. Physical properties of Ni@La₂O₃/SiO₂ and Ni–La₂O₃/SiO₂.

Samples	S _{BET} (m ² g ^{−1})	Pore Volume (cm ³ g ^{−1})	Average Pore Size (nm)	d _{NiO} ^a (nm)		d _{Ni} ^b (nm)	
				By XRD ^c	By TEM ^d	By XRD ^c	By TEM ^d
Ni@La ₂ O ₃ /SiO ₂	19.0	0.21	43.9	N. D. ^e	N. D. ^e	N. D. ^e	3.5 (5)
Ni–La ₂ O ₃ /SiO ₂	24.1	0.17	28.6	8.6	7.8	16.4 (44.6)	(26.7)

^a NiO size in the fresh catalyst. ^b Ni size in the reduced and used catalysts. Data in brackets correspond to the Ni size of used catalyst. ^c Crystallite size determined by XRD using the Scherrer equation. ^d Mean particle size determined by TEM images analysis. ^e The particle in TEM image was too small to be observed, or the peak in XRD pattern was too weak to be used for calculations.

Figure 1 shows the powder XRD patterns of the fresh and reduced catalysts. For the fresh Ni–La₂O₃/SiO₂, the peaks at 2θ = 37.2°, 43.3°, and 62.9° are attributed to NiO [44,45]. The reduced Ni–La₂O₃/SiO₂ showed weak Ni peaks at 44.5° and 51.7° [44,45]. As shown in Table 1, the crystallite size of Ni in reduced Ni–La₂O₃/SiO₂ is 16.4 nm, which is about twice that of NiO in fresh Ni–La₂O₃/SiO₂. This indicates that NiO in the fresh Ni–La₂O₃/SiO₂ catalyst is unstable during the reduction process and sintering. In contrast, there are no obviously NiO peaks found in fresh Ni@La₂O₃/SiO₂ catalyst, and a broad Ni peak at 44.5° is found in reduced Ni@La₂O₃/SiO₂ catalyst. This indicates that Ni particle size in the reduced Ni@La₂O₃/SiO₂ catalyst is smaller than that in the reduced Ni–La₂O₃/SiO₂ catalyst. It should be noted here that no La₂O₃ peak was found in any catalyst. This might be due to the very small La₂O₃ crystals formed not able to detect by XRD, or that the La₂O₃ was in the amorphous phase [37]. The results indicate that La₂O₃ was highly dispersed or amorphous in these catalytic systems. Similar results were reported in the literature [38]. The morphology of La₂O₃ (small particle or amorphous phase) needs to be further confirmed by TEM analysis.

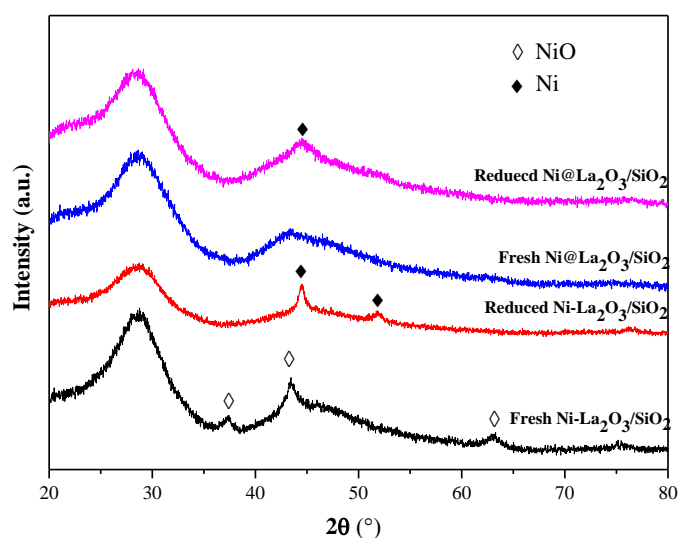


Figure 1. XRD patterns of Ni@La₂O₃/SiO₂ and Ni–La₂O₃/SiO₂ solid catalysts. Reduced catalysts were treated with 20% H₂/Ar at 700 °C for 1.5 h before XRD analysis.

The TEM images of the fresh and reduced catalysts are shown in Figure 2. For the fresh Ni–La₂O₃/SiO₂ catalyst, dark aggregated NiO particles and SiO₂ particles ~20 nm with a smooth surface are shown in Figure 2a, indicating that most of NiO was not loaded onto SiO₂ supported but aggregated instead. The particle size distribution of NiO is displayed in the inset of Figure 2a. The representative high-resolution TEM images in Figure 2b show lattice fringes corresponding to La₂O₃ and NiO, thus illustrating the formation of NiO and La₂O₃ in the fresh Ni–La₂O₃/SiO₂ catalyst.

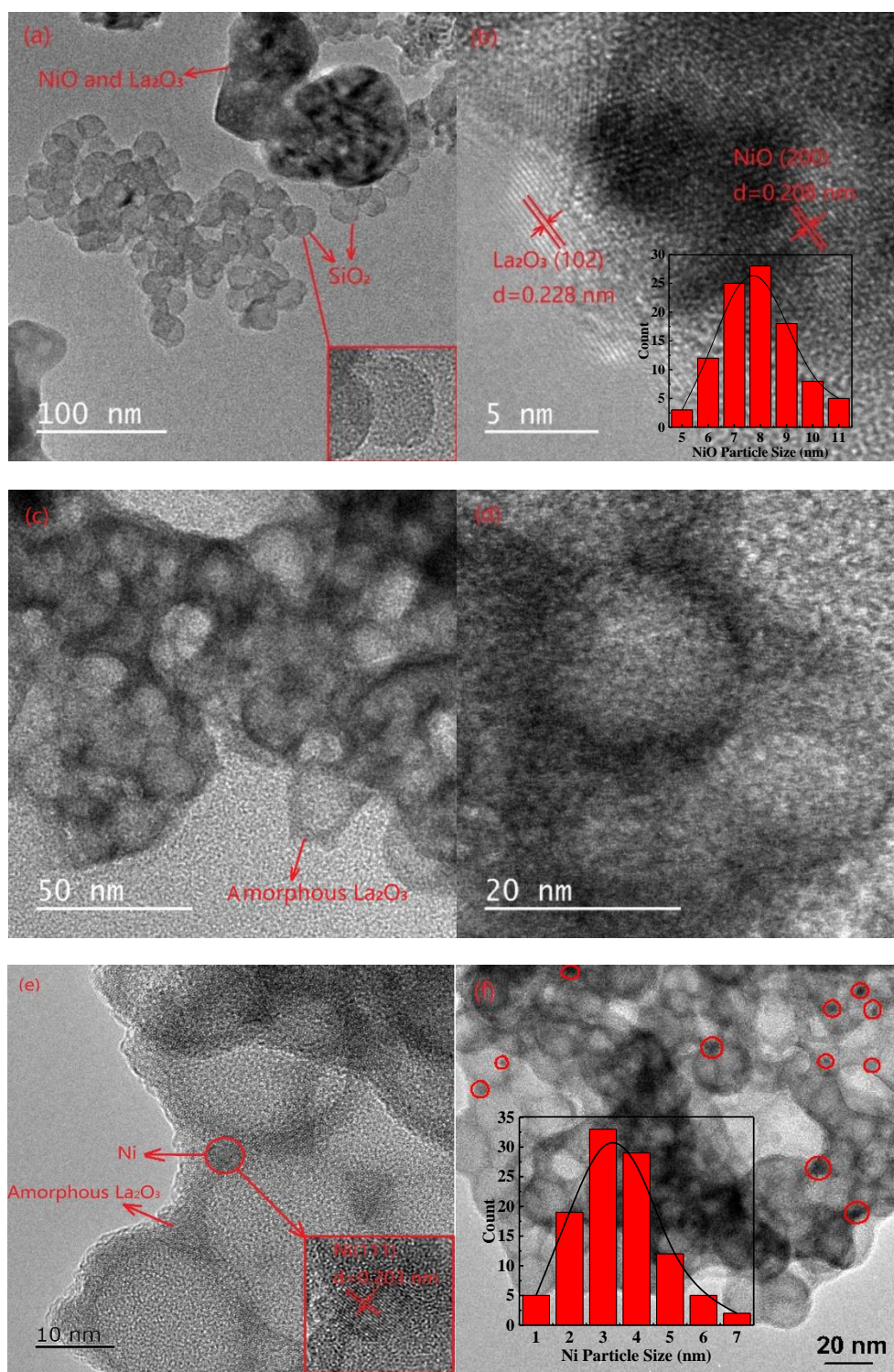


Figure 2. TEM images of Ni@La₂O₃/SiO₂ and Ni-La₂O₃/SiO₂ catalysts: (a,b) fresh Ni-La₂O₃/SiO₂, (c,d) fresh Ni@La₂O₃/SiO₂, and (e,f) reduced Ni@La₂O₃/SiO₂.

Figure 2c,d show TEM images of the fresh Ni@La₂O₃/SiO₂ catalyst. SiO₂ nanospheres are coated with a layer of amorphous La₂O₃, and there are no NiO particles observed, indicating that small NiO particles are highly dispersed on the La₂O₃ coating. A TEM image of the reduced Ni@La₂O₃/SiO₂ catalyst is shown in Figure 2e. As observed, SiO₂ is coated with an amorphous La₂O₃ layer, on which metallic Ni particles are encapsulated within the amorphous La₂O₃ layer. An average Ni particle size

about 3.5 nm was obtained by counting more than 100 Ni particles as shown in Figure 2f. This result is consistent with our previous report of mesoporous Ni–La₂O₃ prepared via colloidal solution combustion method [44].

Combined with TEM and S_{BET} results, it can be concluded that the lower S_{BET} of Ni@La₂O₃/SiO₂ may be due to the fact that the surface of SiO₂ nanoparticles was covered with La₂O₃ and NiO. On the contrary, the SiO₂ nanoparticles in the Ni@La₂O₃/SiO₂ catalyst structure may not be completely covered by La₂O₃ and NiO, and the exposed SiO₂ surface resulted in a slightly larger S_{BET} .

The BF-STEM images and the element distribution profiles of Si, La, and Ni are shown in Figure 3. SiO₂ is surrounded by La₂O₃ and Ni nanoparticles. The signal of Ni is accompanied by the existence of La, but the signal of La is not necessarily accompanied by Ni, indicating that the nickel is encapsulated by La₂O₃. The signal of La₂O₃ is distributed around the signal of silica, indicating that SiO₂ is encapsulated by La₂O₃. The Ni particles are encapsulated by amorphous La₂O₃ and wrapped on silica.

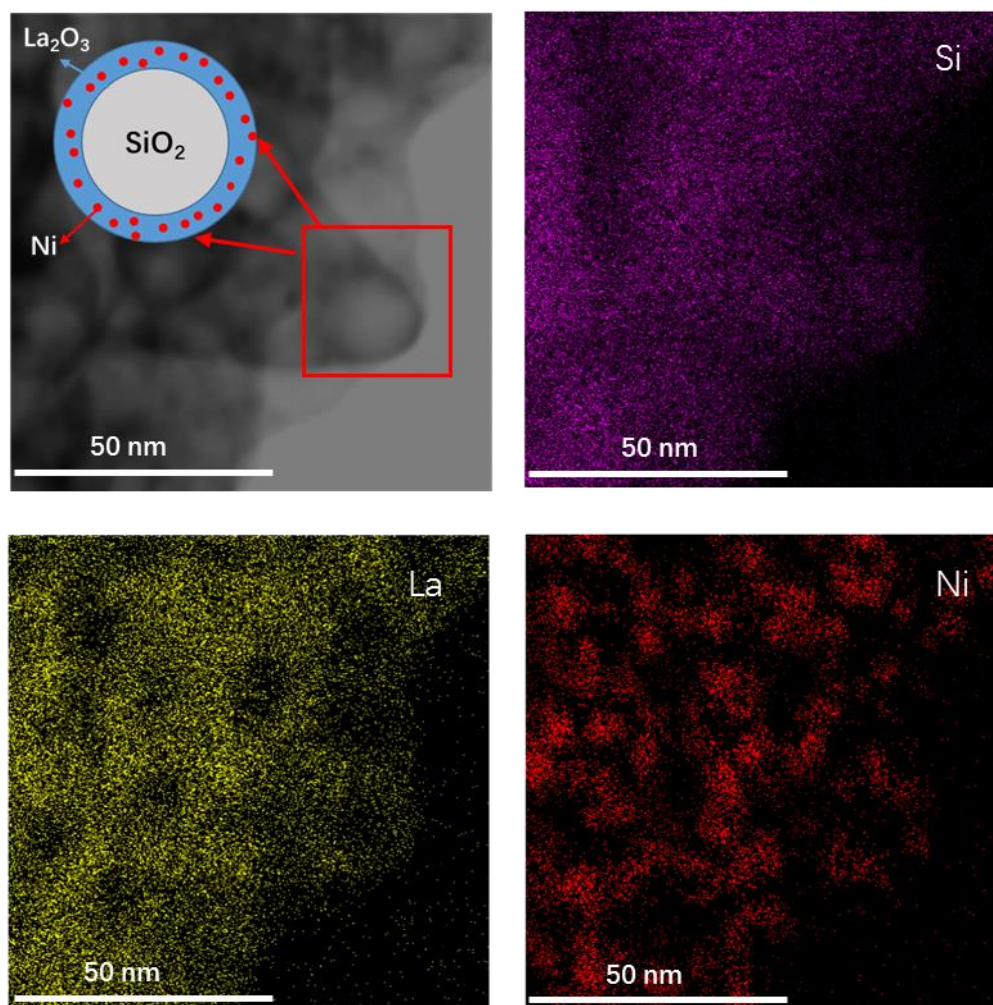


Figure 3. STEM-EDS mapping images of Si, La, and Ni images of Ni@La₂O₃/SiO₂ after reduction.

The H₂-TPR profiles of the catalysts are shown in Figure 4. The Ni–La₂O₃/SiO₂ catalyst exhibits two reduction peaks. The first peak at 340 °C corresponds to the reduction of free NiO [21,39,46]. The second peak at 385 °C corresponds to the reduction of NiO with weak interaction with La₂O₃ or SiO₂ [40,42,47,48]. These results indicate that NiO is weakly interacting or not interacting at all with La₂O₃ or SiO₂ in the Ni–La₂O₃/SiO₂ catalyst.

The Ni@La₂O₃/SiO₂ catalyst displays a broad reduction peak at 615 °C, suggesting that Ni-based species have a strong interaction with the support [42,49]. Li et al. [42] found that the small NiO

particle confined into mesoporous La_2O_3 strongly interacts with La_2O_3 support, resulting in a high reduction temperature for NiO. Also, the $\text{Ni@La}_2\text{O}_3/\text{SiO}_2$ catalyst, which possesses the encapsulated structure of metal Ni by La_2O_3 layer on SiO_2 (in Figure 3a), exhibits high reduction temperatures. Thus, the high reduction temperature at 615 °C is due to the reduction of NiO, which presents strong interactions with the encapsulated La_2O_3 layer.

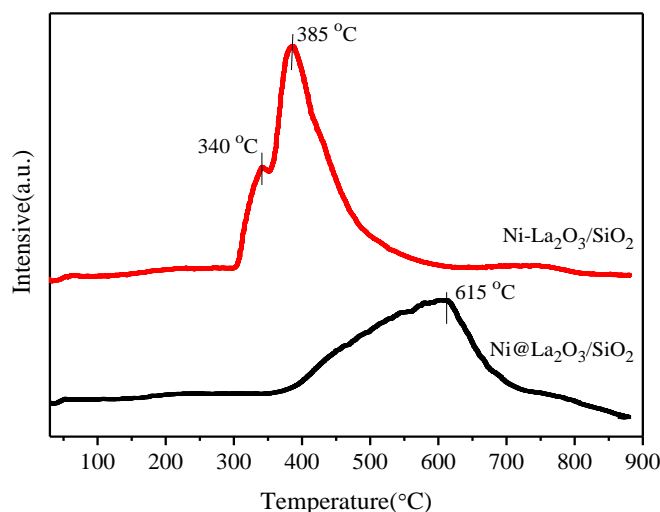


Figure 4. H_2 -TPR traces of $\text{Ni@La}_2\text{O}_3/\text{SiO}_2$ and $\text{Ni-La}_2\text{O}_3/\text{SiO}_2$ catalysts.

2.2. Catalytic Performance Studies

Figure 5 shows results of the catalytic performance tests conducted over the $\text{Ni@La}_2\text{O}_3/\text{SiO}_2$ and $\text{Ni-La}_2\text{O}_3/\text{SiO}_2$ catalysts in the DRM at 700 °C with a weight hourly space velocity (WHSV) of $120,000 \text{ mL g}^{-1} \text{ h}^{-1}$ and after 50 h of reaction. At 700 °C, the thermodynamic equilibrium conversion of CO_2 and CH_4 were 90.2% and 84.4%, respectively. It should be noted that this thermodynamic equilibrium consists of the DRM reaction and reverse water-gas shift reaction (RWGS: $\text{CO}_2 + \text{H}_2 \leftrightarrow \text{CO} + \text{H}_2\text{O}$). As shown in Figure 5a, the CO_2 conversion on the $\text{Ni@La}_2\text{O}_3/\text{SiO}_2$ catalyst is 90% and reached the equilibrium conversion. The CO_2 conversion in the two catalysts are higher than the CH_4 conversion, a result which is mainly due to the RWGS reaction [31]. The $\text{Ni@La}_2\text{O}_3/\text{SiO}_2$ catalyst exhibits stable CO_2 and CH_4 conversions during the DRM reaction period of 50 h. In contrast, the CO_2 and CH_4 conversions of the $\text{Ni-La}_2\text{O}_3/\text{SiO}_2$ catalyst decrease from 75% to 62% and from 63% to 49%, within 50 h, respectively. Therefore, the $\text{Ni@La}_2\text{O}_3/\text{SiO}_2$ catalyst has better activity and stability behavior than the $\text{Ni-La}_2\text{O}_3/\text{SiO}_2$ catalyst during DRM.

As shown in Figure 5b, the H_2/CO ratio is lower than one for both catalysts. This result is mainly due to the RWGS reaction and to a less degree to other side reactions [31], such as the reverse Boudouard reaction ($\text{C} + \text{CO}_2 \leftrightarrow 2 \text{CO}$) [49]. The CO and H_2 yields are shown in Figure 5c,d, respectively. For each catalyst, the CO yield is higher than the H_2 yield. Comparing the two catalysts, the $\text{Ni@La}_2\text{O}_3/\text{SiO}_2$ catalyst exhibits higher H_2 and CO yields than the $\text{Ni-La}_2\text{O}_3/\text{SiO}_2$ catalyst.

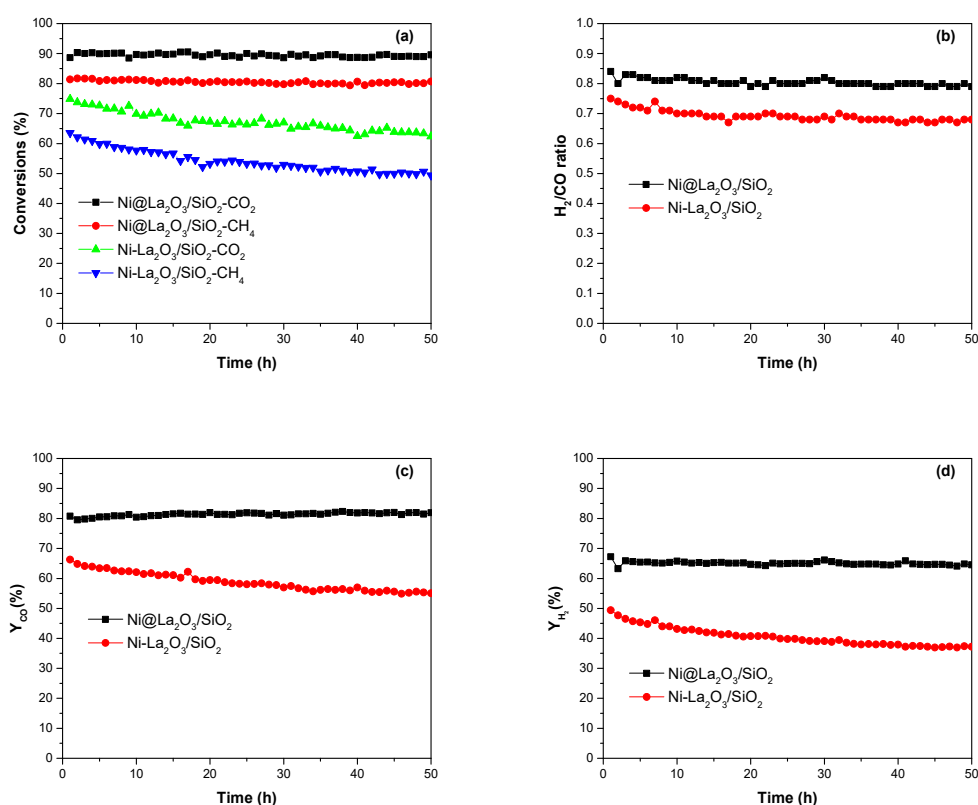


Figure 5. Stability tests performed over the Ni@La₂O₃/SiO₂ and Ni-La₂O₃/SiO₂ catalysts in the dry reforming of methane (DRM). (a) CO₂ and CH₄ conversions, (b) H₂/CO ratio, (c) CO yield, and (d) H₂ yield. Reaction conditions: Total P = 1 atm, CH₄/CO₂/Ar = 15/15/70 (vol%), T = 700 °C, weight hourly space velocity (WHSV) = 120,000 mL g⁻¹ h⁻¹.

No sign of deactivation was observed for the Ni@La₂O₃/SiO₂ catalyst with a WHSV of 120,000 mL g⁻¹ h⁻¹, as shown in Figure 5, and Figure 6 illustrates the effect of WHSV on the catalytic performance of the Ni@La₂O₃/SiO₂ catalyst in the range of 120,000 to 1,200,000 mL g⁻¹ h⁻¹.

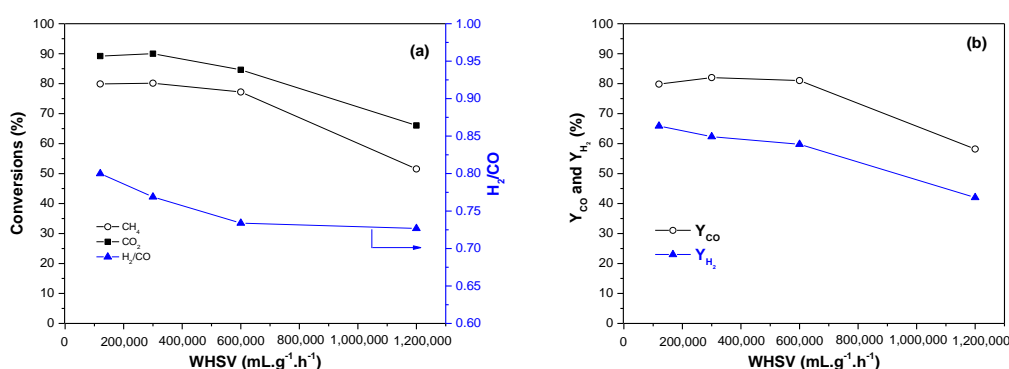


Figure 6. Effect of space velocity on the catalytic performance of Ni@La₂O₃/SiO₂ catalyst. Reaction conditions: P = 1 atm, CH₄/CO₂/Ar = 15/15/70 (vol%), T = 700 °C.

As shown in Figure 6a, in the 120,000–300,000 mL g⁻¹ h⁻¹ range, the CO₂ and CH₄ conversions obviously remain constant. When the WHSV increased to 600,000 mL g⁻¹ h⁻¹, the conversions start to decrease slightly, but the CH₄ conversion is still higher than 70%, suggesting the very good activity of the catalyst. In particular, when the WHSV is increased to 1,200,000 mL g⁻¹ h⁻¹, the conversions of CH₄ and CO₂ are decreased to 51.7% and 65.7%. Accordingly, the CO and H₂ yields show the same trend, which are decreased significantly when the WHSV becomes larger than 600,000 mL g⁻¹ h⁻¹.

This behavior with WHSV is largely related to external mass transport effects established within the catalytic bed.

Figure 7 shows results of the stability test of Ni@La₂O₃/SiO₂ catalyst conducted at a high WHSV of 600,000 mL g⁻¹ h⁻¹. Although the CH₄ and CO₂ conversions are slightly decreased over 80 h of reaction, the CH₄ conversion is still as high as 65% after reaction, indicating the very good activity and stability of the Ni@La₂O₃/SiO₂ catalyst.

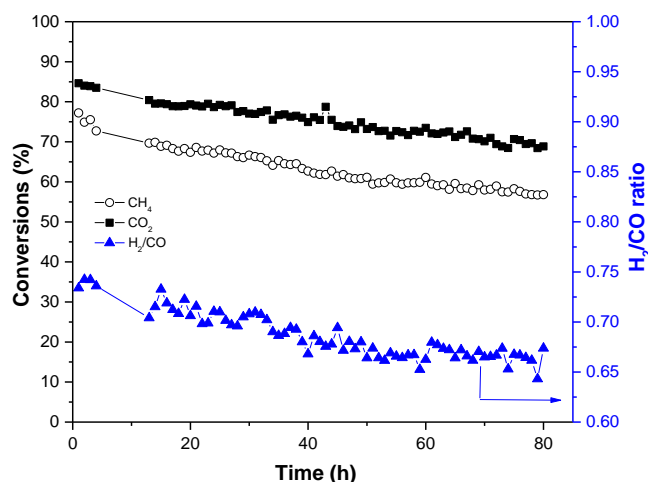


Figure 7. Stability test conducted over the Ni@La₂O₃/SiO₂ catalyst for 80 h at high space velocity. Reaction conditions: P = 1 atm, CH₄/CO₂/Ar = 15/15/70 (vol%), T = 700 °C, WHSV = 600,000 mL g⁻¹ h⁻¹.

Table 2 lists the methane conversion rates obtained over Ni@La₂O₃/SiO₂ and some representative Ni-based catalysts reported in the literature. As listed in Table 2, the CH₄ conversion rate of Ni@La₂O₃/SiO₂ catalyst is five times higher than that of Ni-La₂O₃/SiO₂ catalyst. Although the literature in Table 2 is limited, it appears that the Ni@La₂O₃/SiO₂ catalyst has a significantly better methane conversion rate and coke resistance in the DRM reaction at the conditions applied.

Table 2. Methane conversion and carbon deposition rates of Ni@La₂O₃/SiO₂, Ni-La₂O₃/SiO₂, and recently reported catalysts for the DRM reaction at 700 °C.

	Ni (wt %)	WHSV (mL g _{cat} ⁻¹ h ⁻¹)	X _{CH₄} (%)	CH ₄ Conversion Rate (mmol CH ₄ g _{Ni} ⁻¹ s ⁻¹)	Carbon Deposition Rates (mg C g _{Ni} ⁻¹ h ⁻¹)	Ref.
Ni@La ₂ O ₃ /SiO ₂	6.3	1,200,000	35	12.40 ^a	/	This Work
Ni@La ₂ O ₃ /SiO ₂	6.3	600,000	61	10.10 ^b	0.33 ^d	This Work
Ni-La ₂ O ₃ /SiO ₂	6.3	120,000	49	1.74 ^c	2.60	This Work
Ni/La ₂ O ₃ -LOC	5.7	300,000	23.6	2.31	2.30	[40]
SiO ₂ @Ni@ZrO ₂	8.9	180,000	43.1	3.60	Not detected	[32]
Ni/CeO ₂ -SiO ₂	5	48,000	78.5	2.34	/	[14]
Ni@SiO ₂	3.6	18,000	75	2.33	/	[28]
Ni/LaZr _x O _y	12.7	60,000	55	0.64	0.56	[51]

^a The rate was calculated after reaction for 30 h. ^b The rate was calculated after reaction for 80 h. ^c The rate was calculated after reaction for 50 h. ^d WHSV = 120,000 mL g_{cat}⁻¹ h⁻¹.

2.3. Characterization of Used Catalysts

To measure the amount of deposited carbon on the used catalysts, TG and DTA tests were conducted, and the obtained results are shown in Figure 8a,b. For the used Ni-La₂O₃/SiO₂ catalyst, the weight loss is 11.5 wt% in the range 500–700 °C, and the DTA exhibits an obvious exothermic peak due to the oxidation of deposited carbon. The weight loss of the used Ni@La₂O₃/SiO₂ catalyst was only 1.6 wt% over 50 h in DRM, which is significantly lower than that obtained in the used Ni-La₂O₃/SiO₂ catalyst (11.5 wt% carbon deposition). These results indicate that Ni@La₂O₃/SiO₂ catalyst has a very good resistance to carbon deposition.

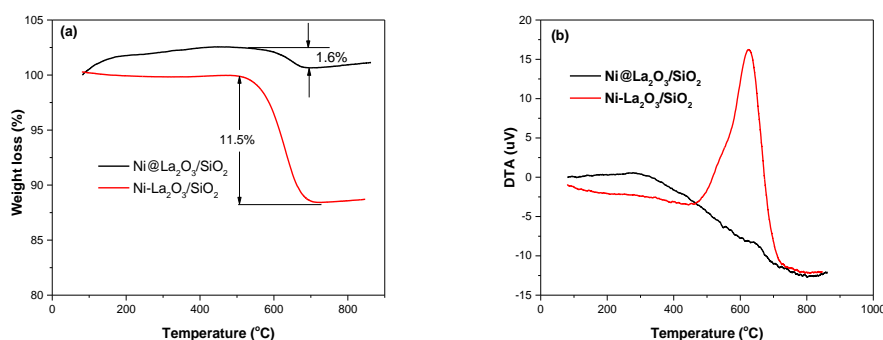


Figure 8. (a) thermogravimetric (TG) and (b) differential thermal analysis (DTA) curves of the used Ni@La₂O₃/SiO₂ and Ni-La₂O₃/SiO₂ catalysts after 50 h of DRM at 700 °C with a WHSV of 120,000 mL g⁻¹ h⁻¹.

The reason for the very good resistance to carbon deposition for the aforementioned catalyst might be partly due to the formed La₂O₃ layer, within which the Ni metallic active sites are well dispersed and less prone to carbon accumulation. As recently reported [52], the Ce_{0.8}Pr_{0.2}O_{2-δ}-supported Ni catalyst prepared by the citrate sol-gel method, due to the presence of mobile active oxygen species in the Ce_{0.8}Pr_{0.2}O_{2-δ} support, largely participates in the carbon removal via gasification to CO(g). Moreover, Ni particles smaller in size can reduce carbon accumulation [53]. Therefore, the good carbon resistance exhibited by Ni@La₂O₃/SiO₂ catalyst seems to be largely related to the smaller nickel particle size and the presence of La₂O₃ coating layer on the Ni particles.

Based on the weight loss range of temperatures ca. 480–730 °C along the exothermic peak, the carbon deposited is composed of whisker carbon and encapsulated graphitic carbon. It should be noted that the encapsulated graphitic carbon is usually responsible for catalyst deactivation [54]. However, the whisker carbon, which possesses hollow structure, has little effect on the active sites of metallic Ni, and therefore is not the main reason for catalyst deactivation.

Figure 9 shows the XRD patterns of the used catalysts. After a 50 h DRM reaction, the used Ni-La₂O₃/SiO₂ catalyst shows an obvious graphitic peak ($2\theta = 26.5^\circ$) [31] and Ni peaks ($2\theta = 44.5^\circ$ and 51.8°) as well. As shown in Table 1, the crystallite size of Ni in the used catalyst increased to 44.6 nm, indicating that Ni particles in the Ni-La₂O₃/SiO₂ catalyst are not stable during the DRM reaction, and large Ni particles and carbon deposition are formed during reaction. The weak Ni diffraction peaks found in the used Ni@La₂O₃/SiO₂ catalyst indicate that Ni particles become smaller after DRM for 50 h. These results indicate that Ni particles in the Ni@La₂O₃/SiO₂ catalyst are more stable than in Ni-La₂O₃/SiO₂ catalyst. In addition, no obvious diffraction peak of graphitic carbon is observed in the used Ni@La₂O₃/SiO₂ catalyst. As proved by the TG-DTA analysis, the amount of carbon deposition (1.6 wt%) is rather small to be detected by powder XRD.

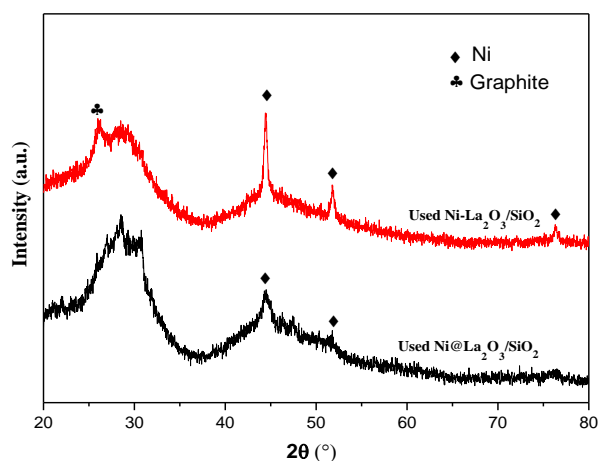


Figure 9. XRD patterns of the used Ni@La₂O₃/SiO₂ and Ni–La₂O₃/SiO₂ catalysts after 50 h of DRM at 700 °C with a WHSV of 120,000 mL g^{−1} h^{−1}.

TEM images of the used catalysts are shown in Figure 10. No whisker carbon was found in the used Ni@La₂O₃/SiO₂ (Figure 10a,b). The Ni mean particle size is about 5 nm, which is slightly larger than that in the reduced Ni@La₂O₃/SiO₂, indicating that the small Ni particles encapsulated into the amorphous La₂O₃ layer are thermally stable and largely contribute to the inhibition of carbon deposition.

As shown in Figure 10, accessible nickel particles (without encapsulation) favor the formation of carbon. Carbon nanofibers and encapsulated graphitic carbon were formed over the used Ni–La₂O₃/SiO₂ catalyst. Methane decomposes on the nickel surface forming atomic hydrogen and carbon, the latter diffusing to free surface sites on the nickel particle to form graphitic carbon (the graphitic carbon peak is precisely seen in Figure 9) [55,56]. As shown in Figure 10c, Ni particles in the used Ni–La₂O₃/SiO₂ catalyst are in the 10–50 nm range, which is much wider than that found in the used Ni@La₂O₃/SiO₂ catalyst. These results are consistent with the TG and XRD results of the used catalysts. It is mentioned here that deposited carbon can plug the reactor and reduce the lifetime of the catalyst as well. However, in general, the formation of carbon nanofibers does not decrease the exposed Ni surface area of the catalyst, thereby maintaining stable catalytic activity. Ni sintering and the formation of encapsulated carbon can reduce the exposed Ni surface area and thus result in catalyst deactivation.

Based on the Ni@La₂O₃/SiO₂ catalyst structure features, it is reasonable to propose that its excellent activity, stability, and high resistance to carbon deposition are much related to the small Ni particles encapsulated within the amorphous La₂O₃ layer deposited on SiO₂. Chen et al. [38] has prepared Ni–La₂O₃/SiO₂ via one-pot sol-gel method with large specific surface area (190 m² g^{−1}), which exhibited high activity and excellent stability for DRM at 700 °C. However, the rate of deposited carbon on Ni–La₂O₃/SiO₂ was 5.9 mg C g_{cat}^{−1} h^{−1}, which is much higher than that found in the present Ni@La₂O₃/SiO₂ catalyst (0.32 mg C g_{cat}^{−1} h^{−1}). Although the BET surface area of the Ni@La₂O₃/SiO₂ catalyst is relatively low, the amorphous La₂O₃ layer can encapsulate and stabilize the small nickel particles formed, thus resulting in an active and stable Ni@La₂O₃/SiO₂ catalyst. Based on the XRD, TEM, and TPR results, it can be concluded that the formed Ni@La₂O₃/SiO₂ catalyst structure cannot only stabilize small nickel particles and reduce carbon accumulation, but also provides more interface between Ni and La₂O₃. The latter can promote CO₂ activation on oxygen vacant sites and on highly basic nature oxygen sites (lanthana oxycarbonates), which was found to be beneficial for inhibiting carbon deposition and enhancing catalytic performance [42,57].

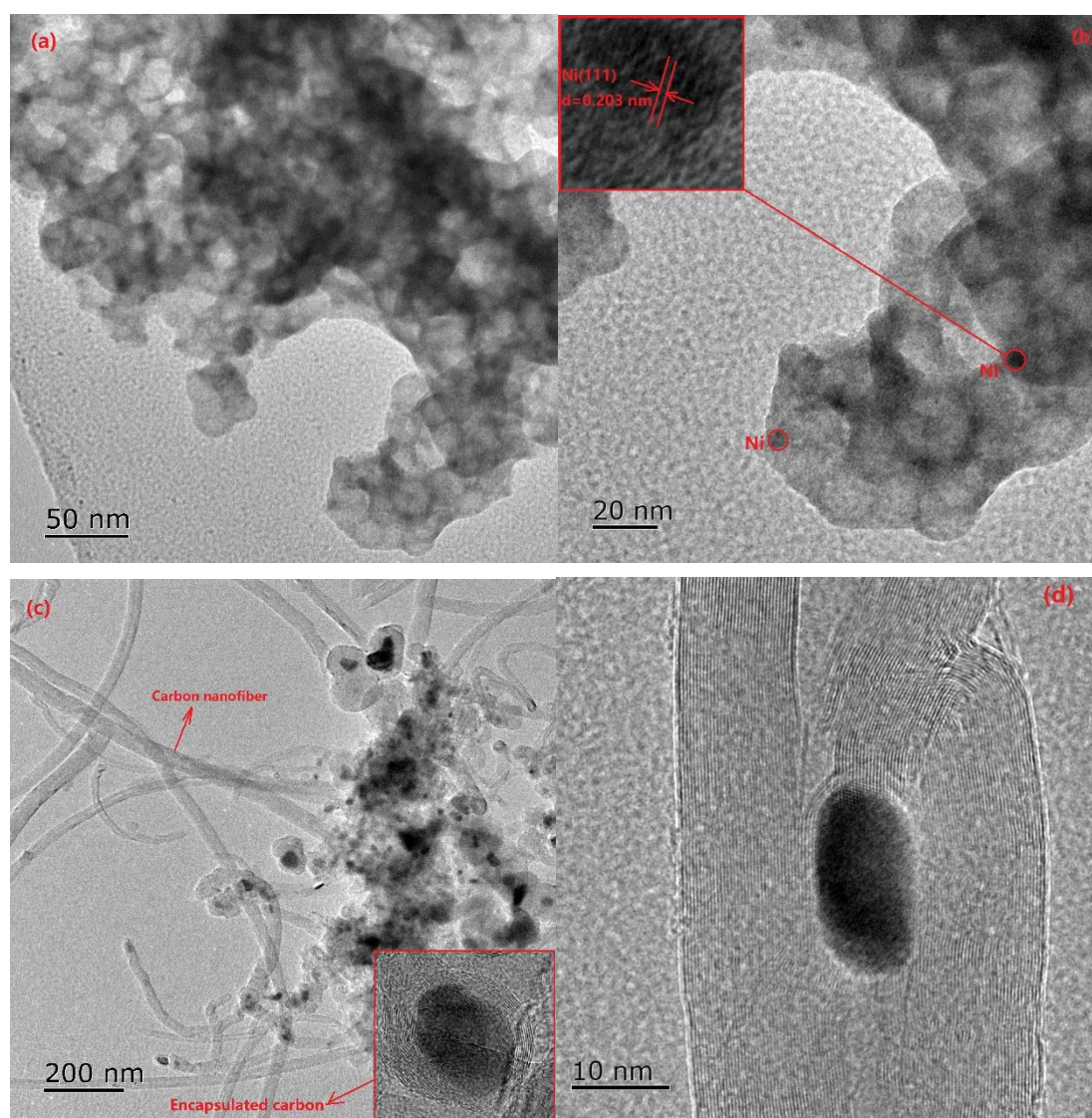


Figure 10. TEM images of the used (a,b) Ni@La₂O₃/SiO₂ and (c,d) Ni-La₂O₃/SiO₂ catalysts after 50 h of DRM at 700 °C with a WHSV of 120,000 mL g⁻¹ h⁻¹.

Even though the encapsulation of nanometal particles in core-shell or yolk-shell structures for stabilizing nanometal particles and inhibiting carbon deposition for high-temperature reactions have been reported in the literature, encapsulated metal catalyst using an inert shell, such as SiO₂, can always result in lower activity due to the blockage of active sites [58]. There is still research demand to develop a simple method for preparing encapsulated metal catalysts with high activity. In this work, a simple colloidal solution combustion method was used to prepare a Ni@La₂O₃/SiO₂ catalyst with small Ni particles encapsulated within amorphous La₂O₃ layer supported on SiO₂. The Ni@La₂O₃/SiO₂ catalyst obtained exhibited high activity and low carbon deposition rate for the DRM reaction conducted at 700 °C and using 15% CH₄, CH₄/CO₂ = 1. This method is a simple approach that can be widely applied for the preparation of encapsulated metal catalysts.

3. Materials and Methods

3.1. Synthesis of Catalysts

A Ni@La₂O₃/SiO₂ catalyst with Ni encapsulated within amorphous La₂O₃ layer on SiO₂ support was prepared via a one-pot colloidal solution combustion method. La(NO₃)₃·6H₂O (2.39 g),

Ni(NO₃)₂·6H₂O (0.50 g), and glycine (0.60 g) were added in deionized water (6.30 mL). After 20 min of ultrasonic stirring, 1.26 mL of aqueous colloidal SiO₂ LUDOX TMA (34 wt%, diameter of 22 nm; Sigma-Aldrich, St. Louis, MO, USA) was added to the solution. After 30 min of ultrasonic stirring, the solution was heated to 250 °C. After a few minutes of heating, glycine and nitrate began to react to form metal oxides and release a large amount of gas. In the combustion reaction, glycine and nitrate were used as the fuel and oxidizer, respectively. After the solid was formed, it was calcined at 700 °C for 4 h, and the Ni@La₂O₃/SiO₂ catalyst was obtained. The weight contents of Ni and La₂O₃ in this catalyst were 6.7% and 60.0%, respectively. For comparison, a Ni–La₂O₃/SiO₂ catalyst with the same Ni and La₂O₃ contents was prepared using the same method without adding glycine.

3.2. Characterization of Catalysts

N₂ adsorption/desorption curves were obtained using an Autosorb-iQ analyzer (Quantachrome Instruments, Boynton Beach, FL, USA) at −196 °C, to quantify the specific surface area, pore size distribution/mean pore size, and pore volume of the catalysts. The crystal structure of the catalysts was determined by powder X-ray diffraction (XRD). The spectra were collected using a Rigaku-Miniflex 6 (Rigaku Corporation, Tokyo, Japan) powder X-ray diffractometer equipped with CuKα (λ = 0.15406 nm), between 20° and 80° (2θ) at a scanning speed of 10° min^{−1}.

H₂-temperature programmed reduction (H₂-TPR) was applied on a TP-5080 multifunctional adsorption apparatus (Xianquan, Tianjin, China) in 5% H₂/Ar gas mixture with a heating rate of 10 °C min^{−1}. Transmission electron microscopy (TEM) was performed on a Tecnai G2 F20 microscope (FEI Company, Hillsboro, OR, USA), to directly observe the morphology and size of Ni particles and of deposited carbon after DRM. To determine the amount of carbon accumulation of the used catalysts, thermogravimetric (TG) and differential thermal analysis (DTA) were conducted on an HCT-1 TG thermal analyzer (Henven Scientific Instruments, Beijing, China).

3.3. Catalysts Performance Evaluation for the DRM Reaction

The catalytic performance of the Ni-based solids was evaluated at atmospheric pressure in a fixed-bed tubular quartz reactor (internal diameter 8 mm, length 300 mm). The total flow rate of reaction gases was 100 mL min^{−1} and the amount of catalyst used was in the 5–50 mg range. The corresponding WHSV was in the 120,000–1,200,000 mL g^{−1} h^{−1} range. CH₄, CO₂, H₂, and Ar (99.999% purity) were purchased from Shanghai Maytor special Gas Co. Ltd. These gases contained less than 1 ppm of water vapor and were used without further purification. Before reaction, the catalyst was in-situ reduced in 20% H₂/Ar gas mixture at 700 °C for 1.5 h. The reaction gases of CO₂, CH₄, and Ar at a molar ratio of 15/15/70 (vol%), were introduced into the reactor at 700 °C, and Ar gas was used as the internal standard. The gas effluent was analyzed using two on-line gas chromatographs of G5 (Beijing Purkinje General Instrument Co., Ltd., Beijing, China). One chromatograph used hydrogen as a carrier gas to detect Ar, CO, CH₄, and CO₂. Another chromatograph used N₂ as a carrier gas to detect H₂.

The CO₂ conversion (X_{CO2}), CH₄ conversion (X_{CH4}) and the H₂/CO gas product ratio were calculated based on the following Equations (1)–(3):

$$X_{\text{CO}_2} = \frac{[\text{CO}_2]_{\text{in}} - [\text{CO}_2]_{\text{out}}}{[\text{CO}_2]_{\text{in}}} \times 100\% \quad (2)$$

$$X_{\text{CH}_4} = \frac{[\text{CH}_4]_{\text{in}} - [\text{CH}_4]_{\text{out}}}{[\text{CH}_4]_{\text{in}}} \times 100\% \quad (3)$$

$$\text{H}_2/\text{CO} = \frac{[\text{H}_2]_{\text{out}}}{[\text{CO}]_{\text{out}}} \quad (4)$$

where [x]_{in} and [x]_{out} represent the mole fraction of x gaseous species in the inlet feed and outlet from reactor gas mixture, respectively.

The H₂ and CO product yields were calculated based on the following Equations (4) and (5):

$$Y_{\text{H}_2} = \frac{[\text{H}_2]_{\text{out}}}{2[\text{CH}_4]_{\text{in}}} \times 100\% \quad (5)$$

$$Y_{\text{CO}} = \frac{[\text{CO}]_{\text{out}}}{[\text{CH}_4]_{\text{in}} + [\text{CO}_2]_{\text{in}}} \times 100\% \quad (6)$$

4. Conclusions

In this study, we prepared a Ni@La₂O₃/SiO₂ catalyst with encapsulated Ni nanoparticles via the colloidal solution combustion method tested for the DRM reaction at 700 °C. In the Ni@La₂O₃/SiO₂ catalyst, small Ni particles were encapsulated within an amorphous La₂O₃ layer, where this was coated on SiO₂. Due to the encapsulated Ni micro-structure, more interface between Ni and La₂O₃ was formed, and the Ni@La₂O₃/SiO₂ catalyst exhibited excellent activity and stability and strong resistance to carbon deposition during DRM reaction. The catalytic performance results indicated that the CH₄ conversion rate of the Ni@La₂O₃/SiO₂ catalyst was five times higher than that of Ni–La₂O₃/SiO₂ catalyst. More importantly, the Ni@La₂O₃/SiO₂ catalyst exhibited excellent catalytic stability and only a slight deactivation for 80 h on reaction stream. TG-DTA studies revealed that 1.6 wt% carbon was deposited on the Ni@La₂O₃/SiO₂ catalyst after 50 h of DRM, which was much lower than that of 11.5 wt% obtained on the Ni–La₂O₃/SiO₂ catalyst.

Author Contributions: Conceptualization, L.W.; data curation, L.W. and R.H.; formal analysis, L.W., H.L., D.G. and L.M.; funding acquisition, L.W. and H.L.; investigation, L.W., R.H. and Z.Z.; writing—original draft, L.W. and R.H.; writing—review and editing, H.L., Q.W., D.G. and H.T. All authors have read and agreed to the published version of the manuscript.

Funding: This research was funded by the Fundamental Research Funds for Zhejiang Provincial Universities and Research Institutes (No. 2019JZ00003), the Science and Technology Foundation of Zhoushan (No. 2018C21013), the Scientific Research Project of Zhejiang Education Department (No. Y201636192), and the university students' innovation program of Zhejiang province (No. 2018R411009).

Conflicts of Interest: The authors declare no conflict of interest.

References

1. Khodakov, A.Y.; Chu, W.; Fongarland, P. Advances in the Development of Novel Cobalt Fischer–Tropsch Catalysts for Synthesis of Long-Chain Hydrocarbons and Clean Fuels. *Chem. Rev.* **2007**, *107*, 1692–1744. [[CrossRef](#)]
2. Abdurashheed, A.; Jalil, A.A.; Gambo, Y.; Ibrahim, M.; Hambali, H.U.; Shahul Hamid, M.Y. A review on catalyst development for dry reforming of methane to syngas: Recent advances. *Renew. Sustain. Energy Rev.* **2019**, *108*, 175–193. [[CrossRef](#)]
3. Jang, W.-J.; Shim, J.-O.; Kim, H.-M.; Yoo, S.-Y.; Roh, H.-S. A review on dry reforming of methane in aspect of catalytic properties. *Catal. Today* **2019**, *324*, 15–26. [[CrossRef](#)]
4. Aramouni, N.A.K.; Touma, J.G.; Tarboush, B.A.; Zeaiter, J.; Ahmad, M.N. Catalyst design for dry reforming of methane: Analysis review. *Renew. Sustain. Energy Rev.* **2018**, *82*, 2570–2585. [[CrossRef](#)]
5. Ghelamallah, M.; Granger, P. Impact of barium and lanthanum incorporation to supported Pt and Rh on α -Al₂O₃ in the dry reforming of methane. *Fuel* **2012**, *97*, 269–276. [[CrossRef](#)]
6. De Miguel, S.R.; Vilella, I.M.J.; Maina, S.P.; San José-Alonso, D.; Román-Martínez, M.C.; Illán-Gómez, M.J. Influence of Pt addition to Ni catalysts on the catalytic performance for long term dry reforming of methane. *Appl. Catal. A Gen.* **2012**, *435*, 10–18. [[CrossRef](#)]
7. Crisafulli, C.; Scirè, S.; Maggiore, R.; Minicò, S.; Galvagno, S. CO₂ reforming of methane over Ni–Ru and Ni–Pd bimetallic catalysts. *Catal. Lett.* **1999**, *59*, 21–26. [[CrossRef](#)]
8. Wang, Y.; Yao, L.; Wang, S.; Mao, D.; Hu, C. Low-temperature catalytic CO₂ dry reforming of methane on Ni-based catalysts: A review. *Fuel Process. Technol.* **2018**, *169*, 199–206. [[CrossRef](#)]

9. Abdullah, B.; Abd Ghani, N.A.; Vo, D.-V.N. Recent advances in dry reforming of methane over Ni-based catalysts. *J. Clean. Prod.* **2017**, *162*, 170–185. [[CrossRef](#)]
10. Zhang, G.; Liu, J.; Xu, Y.; Sun, Y. A review of CH₄–CO₂ reforming to synthesis gas over Ni-based catalysts in recent years (2010–2017). *Int. J. Hydrog. Energy* **2018**, *43*, 15030–15054. [[CrossRef](#)]
11. Xie, T.; Shi, L.; Zhang, J.; Zhang, D. Immobilizing Ni nanoparticles to mesoporous silica with size and location control via a polyol-assisted route for coking- and sintering-resistant dry reforming of methane. *Chem. Commun.* **2014**, *50*, 7250–7253. [[CrossRef](#)] [[PubMed](#)]
12. Zhang, Q.; Zhang, T.; Shi, Y.; Zhao, B.; Wang, M.; Liu, Q.; Wang, J.; Long, K.; Duan, Y.; Ning, P. A sintering and carbon-resistant Ni-SBA-15 catalyst prepared by solid-state grinding method for dry reforming of methane. *J. CO₂ Util.* **2017**, *17*, 10–19. [[CrossRef](#)]
13. Djinić, P.; Osojnik Črnivec, I.G.; Erjavec, B.; Pintar, A. Influence of active metal loading and oxygen mobility on coke-free dry reforming of Ni–Co bimetallic catalysts. *Appl. Catal. B Environ.* **2012**, *125*, 259–270. [[CrossRef](#)]
14. Yan, X.; Hu, T.; Liu, P.; Li, S.; Zhao, B.; Zhang, Q.; Jiao, W.; Chen, S.; Wang, P.; Lu, J.; et al. Highly efficient and stable Ni/CeO₂-SiO₂ catalyst for dry reforming of methane: Effect of interfacial structure of Ni/CeO₂ on SiO₂. *Appl. Catal. B Environ.* **2019**, *246*, 221–231. [[CrossRef](#)]
15. Luisetto, I.; Tuti, S.; Battocchio, C.; Lo Mastro, S.; Sodo, A. Ni/CeO₂-Al₂O₃ catalysts for the dry reforming of methane: The effect of CeAlO₃ content and nickel crystallite size on catalytic activity and coke resistance. *Appl. Catal. A Gen.* **2015**, *500*, 12–22. [[CrossRef](#)]
16. Ay, H.; Üner, D. Dry reforming of methane over CeO₂ supported Ni, Co and Ni–Co catalysts. *Appl. Catal. B Environ.* **2015**, *179*, 128–138. [[CrossRef](#)]
17. Gould, T.D.; Izar, A.; Weimer, A.W.; Falconer, J.L.; Medlin, J.W. Stabilizing Ni Catalysts by Molecular Layer Deposition for Harsh, Dry Reforming Conditions. *ACS Catal.* **2014**, *4*, 2714–2717. [[CrossRef](#)]
18. Kim, J.-H.; Suh, D.J.; Park, T.-J.; Kim, K.-L. Effect of metal particle size on coking during CO₂ reforming of CH₄ over Ni–alumina aerogel catalysts. *Appl. Catal. A Gen.* **2000**, *197*, 191–200. [[CrossRef](#)]
19. Abdel Karim Aramouni, N.; Zeaiter, J.; Kwapinski, W.; Ahmad, M.N. Thermodynamic analysis of methane dry reforming: Effect of the catalyst particle size on carbon formation. *Energy Convers. Manag.* **2017**, *150*, 614–622. [[CrossRef](#)]
20. Han, J.W.; Park, J.S.; Choi, M.S.; Lee, H. Uncoupling the size and support effects of Ni catalysts for dry reforming of methane. *Appl. Catal. B Environ.* **2017**, *203*, 625–632. [[CrossRef](#)]
21. Zhang, Q.; Tang, T.; Wang, J.; Sun, M.; Wang, H.; Sun, H.; Ning, P. Facile template-free synthesis of Ni-SiO₂ catalyst with excellent sintering- and coking-resistance for dry reforming of methane. *Catal. Commun.* **2019**, *131*, 105782. [[CrossRef](#)]
22. Kawi, S.; Kathiraser, Y.; Ni, J.; Oemar, U.; Li, Z.; Saw, E.T. Progress in Synthesis of Highly Active and Stable Nickel-Based Catalysts for Carbon Dioxide Reforming of Methane. *ChemSusChem* **2015**, *8*, 3556–3575. [[CrossRef](#)] [[PubMed](#)]
23. Tian, H.; Li, X.; Zeng, L.; Gong, J. Recent Advances on the Design of Group VIII Base-Metal Catalysts with Encapsulated Structures. *ACS Catal.* **2015**, *5*, 4959–4977. [[CrossRef](#)]
24. Liu, W.; Li, L.; Zhang, X.; Wang, Z.; Wang, X.; Peng, H. Design of Ni-ZrO₂@SiO₂ catalyst with ultra-high sintering and coking resistance for dry reforming of methane to prepare syngas. *J. CO₂ Util.* **2018**, *27*, 297–307. [[CrossRef](#)]
25. Li, Z.; Jiang, B.; Wang, Z.; Kawi, S. High carbon resistant Ni@Ni phyllosilicate@SiO₂ core shell hollow sphere catalysts for low temperature CH₄ dry reforming. *J. CO₂ Util.* **2018**, *27*, 238–246. [[CrossRef](#)]
26. Zhang, L.; Wang, F.; Zhu, J.; Han, B.; Fan, W.; Zhao, L.; Cai, W.; Li, Z.; Xu, L.; Yu, H.; et al. CO₂ reforming with methane reaction over Ni@SiO₂ catalysts coupled by size effect and metal-support interaction. *Fuel* **2019**, *256*, 115954. [[CrossRef](#)]
27. Zhao, X.; Li, H.; Zhang, J.; Shi, L.; Zhang, D. Design and synthesis of NiCe@m-SiO₂ yolk-shell framework catalysts with improved coke- and sintering-resistance in dry reforming of methane. *Int. J. Hydrog. Energy* **2016**, *41*, 2447–2456. [[CrossRef](#)]
28. Wang, F.; Han, B.; Zhang, L.; Xu, L.; Yu, H.; Shi, W. CO₂ reforming with methane over small-sized Ni@SiO₂ catalysts with unique features of sintering-free and low carbon. *Appl. Catal. B Environ.* **2018**, *235*, 26–35. [[CrossRef](#)]

29. Wang, C.; Jie, X.; Qiu, Y.; Zhao, Y.; Al-Megren, H.A.; Alshihri, S.; Edwards, P.P.; Xiao, T. The importance of inner cavity space within Ni@SiO₂ nanocapsule catalysts for excellent coking resistance in the high-space-velocity dry reforming of methane. *Appl. Catal. B Environ.* **2019**, *259*, 118019. [[CrossRef](#)]
30. Zhang, J.; Li, F. Coke-resistant Ni@SiO₂ catalyst for dry reforming of methane. *Appl. Catal. B Environ.* **2015**, *176*, 513–521. [[CrossRef](#)]
31. Das, S.; Ashok, J.; Bian, Z.; Dewangan, N.; Wai, M.H.; Du, Y.; Borgna, A.; Hidajat, K.; Kawi, S. Silica–Ceria sandwiched Ni core–shell catalyst for low temperature dry reforming of biogas: Coke resistance and mechanistic insights. *Appl. Catal. B Environ.* **2018**, *230*, 220–236. [[CrossRef](#)]
32. Dou, J.; Zhang, R.; Hao, X.; Bao, Z.; Wu, T.; Wang, B.; Yu, F. Sandwiched SiO₂@Ni@ZrO₂ as a coke resistant nanocatalyst for dry reforming of methane. *Appl. Catal. B Environ.* **2019**, *254*, 612–623. [[CrossRef](#)]
33. Li, K.; He, F.; Yu, H.; Wang, Y.; Wu, Z. Theoretical study on the reaction mechanism of carbon dioxide reforming of methane on La and La₂O₃ modified Ni (1 1 1) surface. *J. Catal.* **2018**, *364*, 248–261. [[CrossRef](#)]
34. Sierra Gallego, G.; Batiot-Dupeyrat, C.; Barrault, J.; Mondragón, F. Dual Active-Site Mechanism for Dry Methane Reforming over Ni/La₂O₃ Produced from LaNiO₃ Perovskite. *Ind. Eng. Chem. Res.* **2008**, *47*, 9272–9278. [[CrossRef](#)]
35. Zhang, Z.; Verykios, X.E.; MacDonald, S.M.; Affrossman, S. Comparative Study of Carbon Dioxide Reforming of Methane to Synthesis Gas over Ni/La₂O₃ and Conventional Nickel-Based Catalysts. *J. Phys. Chem.* **1996**, *100*, 744–754. [[CrossRef](#)]
36. Charisiou, N.D.; Tzounis, L.; Sebastian, V.; Hinder, S.J.; Baker, M.A.; Polychronopoulou, K.; Goula, M.A. Investigating the correlation between deactivation and the carbon deposited on the surface of Ni/Al₂O₃ and Ni/La₂O₃-Al₂O₃ catalysts during the biogas reforming reaction. *Appl. Surf. Sci.* **2019**, *474*, 42–56. [[CrossRef](#)]
37. Mo, W.; Ma, F.; Ma, Y.; Fan, X. The optimization of Ni–Al₂O₃ catalyst with the addition of La₂O₃ for CO₂–CH₄ reforming to produce syngas. *Int. J. Hydrog. Energy* **2019**, *44*, 24510–24524. [[CrossRef](#)]
38. Chen, C.; Wang, X.; Zhang, L.; Zou, X.; Ding, W.; Lu, X. Synthesis of mesoporous Ni–La₂O₃/SiO₂ by ploy(ethylene glycol)-assisted sol-gel route as highly efficient catalysts for dry reforming of methane with a H₂/CO ratio of unity. *Catal. Commun.* **2017**, *94*, 38–41. [[CrossRef](#)]
39. Cheng, H.; Li, G.; Zhao, H.; Lu, X.; Xu, Q.; Tao, W. Effects of preparation technique and lanthana doping on Ni/La₂O₃-ZrO₂ catalysts for hydrogen production by CO₂ reforming of coke oven gas. *Catal. Today* **2018**, *318*, 23–31. [[CrossRef](#)]
40. Li, X.; Li, D.; Tian, H.; Zeng, L.; Zhao, Z.-J.; Gong, J. Dry reforming of methane over Ni/La₂O₃ nanorod catalysts with stabilized Ni nanoparticles. *Appl. Catal. B Environ.* **2017**, *202*, 683–694. [[CrossRef](#)]
41. Xu, L.; Liu, W.; Zhang, X.; Tao, L.; Xia, L.; Xu, X.; Song, J.; Zhou, W.; Fang, X.; Wang, X. Ni/La₂O₃ Catalysts for Dry Reforming of Methane: Insights into the Factors Improving the Catalytic Performance. *ChemCatChem* **2019**, *11*, 2887–2899. [[CrossRef](#)]
42. Li, K.; Chang, X.; Pei, C.; Li, X.; Chen, S.; Zhang, X.; Assabumrungrat, S.; Zhao, Z.-J.; Zeng, L.; Gong, J. Ordered mesoporous Ni/La₂O₃ catalysts with interfacial synergism towards CO₂ activation in dry reforming of methane. *Appl. Catal. B Environ.* **2019**, *259*, 118092. [[CrossRef](#)]
43. Voskanyan, A.A.; Chan, K.-Y.; Li, C.-Y.V. Colloidal Solution Combustion Synthesis: Toward Mass Production of a Crystalline Uniform Mesoporous CeO₂ Catalyst with Tunable Porosity. *Chem. Mater.* **2016**, *28*, 2768–2775.
44. Tang, G.; Gong, D.; Liu, H.; Wang, L. Highly Loaded Mesoporous Ni–La₂O₃ Catalyst Prepared by Colloidal Solution Combustion Method for CO₂ Methanation. *Catalysts* **2019**, *9*, 442. [[CrossRef](#)]
45. Wang, L.; Liu, H.; Ye, H.; Hu, R.; Yang, S.; Tang, G.; Li, K.; Yang, Y. Vacuum Thermal Treated Ni–CeO₂/SBA-15 Catalyst for CO₂ Methanation. *Nanomaterials* **2018**, *8*, 759. [[CrossRef](#)]
46. Zhao, B.; Yao, Y.; Shi, H.; Yang, F.; Jia, X.; Liu, P.; Ma, X. Preparation of Ni/SiO₂ catalyst via novel plasma-induced micro-combustion method. *Catal. Today* **2019**, *337*, 28–36. [[CrossRef](#)]
47. Wang, M.; Zhang, Q.; Zhang, T.; Wang, Y.; Wang, J.; Long, K.; Song, Z.; Liu, X.; Ning, P. Facile one-pot synthesis of highly dispersed Ni nanoparticles embedded in HMS for dry reforming of methane. *Chem. Eng. J.* **2017**, *313*, 1370–1381. [[CrossRef](#)]
48. Garbarino, G.; Wang, C.; Valsamakis, I.; Chitsazan, S.; Riani, P.; Finocchio, E.; Flytzani-Stephanopoulos, M.; Busca, G. A study of Ni/Al₂O₃ and Ni–La/Al₂O₃ catalysts for the steam reforming of ethanol and phenol. *Appl. Catal. B Environ.* **2015**, *174–175*, 21–34. [[CrossRef](#)]
49. Xu, Y.; Lin, Q.; Liu, B.; Jiang, F.; Xu, Y.; Liu, X. A Facile Fabrication of Supported Ni/SiO₂ Catalysts for Dry Reforming of Methane with Remarkably Enhanced Catalytic Performance. *Catalysts* **2019**, *9*, 183. [[CrossRef](#)]

50. Osaki, T.; Mori, T. Role of Potassium in Carbon-Free CO₂ Reforming of Methane on K-Promoted Ni/Al₂O₃ Catalysts. *J. Catal.* **2001**, *204*, 89–97. [[CrossRef](#)]
51. Le Saché, E.; Pastor-Pérez, L.; Watson, D.; Sepúlveda-Escribano, A.; Reina, T.R. Ni stabilised on inorganic complex structures: Superior catalysts for chemical CO₂ recycling via dry reforming of methane. *Appl. Catal. B Environ.* **2018**, *236*, 458–465. [[CrossRef](#)]
52. Vasiliades, M.A.; Damaskinos, C.M.; Kyprianou, K.K.; Kollia, M.; Efstathiou, A.M. The effect of Pt on the carbon pathways in the dry reforming of methane over Ni-Pt/Ce_{0.8}Pr_{0.2}O_{2-δ} catalyst. *Catal. Today* **2019**, in press. [[CrossRef](#)]
53. Chai, Y.; Fu, Y.; Feng, H.; Kong, W.; Yuan, C.; Pan, B.; Zhang, J.; Sun, Y. A Nickel-Based Perovskite Catalyst with a Bimodal Size Distribution of Nickel Particles for Dry Reforming of Methane. *ChemCatChem* **2018**, *10*, 2078–2086. [[CrossRef](#)]
54. Vasiliades, M.A.; Djinović, P.; Davlyatova, L.F.; Pintar, A.; Efstathiou, A.M. Origin and reactivity of active and inactive carbon formed during DRM over Ni/Ce_{0.38}Zr_{0.62}O_{2-δ} studied by transient isotopic techniques. *Catal. Today* **2018**, *299*, 201–211. [[CrossRef](#)]
55. Torres, D.; Pinilla, J.L.; Suelves, I. Co-, Cu- and Fe-Doped Ni/Al₂O₃ Catalysts for the Catalytic Decomposition of Methane into Hydrogen and Carbon Nanofibers. *Catalysts* **2018**, *8*, 300. [[CrossRef](#)]
56. Torres, D.; Pinilla, J.L.; Suelves, I. Screening of Ni-Cu bimetallic catalysts for hydrogen and carbon nanofilaments production via catalytic decomposition of methane. *Appl. Catal. A Gen.* **2018**, *559*, 10–19. [[CrossRef](#)]
57. Vasiliades, M.A.; Makri, M.M.; Djinović, P.; Erjavec, B.; Pintar, A.; Efstathiou, A.M. Dry reforming of methane over 5 wt% Ni/Ce_{1-x}Pr_xO_{2-δ} catalysts: Performance and characterisation of active and inactive carbon by transient isotopic techniques. *Appl. Catal. B Environ.* **2016**, *197*, 168–183. [[CrossRef](#)]
58. Cao, A.; Lu, R.; Vesper, G. Stabilizing metal nanoparticles for heterogeneous catalysis. *Phys. Chem. Chem. Phys.* **2010**, *12*, 13499–13510. [[CrossRef](#)]



© 2019 by the authors. Licensee MDPI, Basel, Switzerland. This article is an open access article distributed under the terms and conditions of the Creative Commons Attribution (CC BY) license (<http://creativecommons.org/licenses/by/4.0/>).